DOI: 10.1002/ejic.200600842

Reticular Nickel Microwires with Assembled Nanostructures: Synthesis, Magnetism and Catalysis for the Growth of Carbon Nanotubes

Xiaomin Ni,[a] Qingbiao Zhao,[a] Yongfeng Zhang,[b] and Huagui Zheng*[a]

Keywords: Nickel / Nanostructures / Chemical reduction / Crystal growth

Reticular nickel microwires assembled from different-shaped building blocks are fabricated by a simple, one-pot method in the absence of any surfactants or external magnetic field. The synthetic process involves the chemical reduction of a nickel complex with hydrazine under controlled reaction conditions. Our strategy focuses on the modulation of the reaction rate to control the shape of the subunits and their spontaneous assembly behavior, which avoids the need for surfactants or an external force. The nickel wires can be reproducibly created with the assistance of various complexants, such as citrate, tartrate, lactate, ethylenediamine, triethanolamine and diethanolamine, which proves the generality of this method. These nickel wires show variable magnetic properties and catalysis for the growth of carbon nanotubes in pyrolyzing acetone due to the nature of their microstructures.

Introduction

Assembled nanostructures have attracted considerable interest from materials scientists due to their potential applications in nanodevices.[1] In particular, magnetic assemblies have received more attention due to their unique properties and uses in electronic, magnetic, and biomedical applications, amongst others.[2] Generally, there are two routes for the assembly of magnetic nanoparticles into organized structures. The first of these harnesses the spontaneous noncovalent interactions between surfactants or polymer-modified building blocks, including van der Waals forces, π–π interactions, electrostatic forces, and hydrogen bonding.[3] For example, a three-dimensional spherical assembly of magnetite nanoparticles has been fabricated in the presence of ternary surfactant combinations[4] and the assembly of maghemite has been achieved in the presence of a block copolypeptide.[5] In the presence of polymers, monodisperse FePt nanoparticles self-assemble into films with controllable thicknesses and dimensions.[6] In these systems, the content of surfactants or polymers is relatively high, which usually damages their magnetic properties or makes their practical application difficult.[7] The other efficient method for the assembly of magnetic nanoparticles makes use of an external magnetic field. The application of a magnetic field to a suspension of magnetic particles typically produces one-dimensional (1D) chains of particles with their magnetic dipoles aligned head-to-tail and parallel to the magnetic field.[8] For instance, application of an external perpendicular magnetic field to a solution of $CoPt_3$ nanocrystals in toluene drives the formation of 1D microwires,[9] and Fe_3O_4 nanoparticles in the size range 8–12 nm self-assemble into elongated clusters on a GaAs substrate in the presence of a strong magnetic field, with the predominant orientation lengthwise along the field direction.[10] Colloidal nickel nanoparticles self-assemble into nanochains when subjected to a magnetic field with a strength of about 250 G.[11] However, these assemblies always require an external magnetic field to remain stable, and when the external magnetic field is removed they become unstable.[12] Currently, it is still challenging to explore simple and convenient approaches for the synthesis of assembled nanostructures.

Nanosized particles of nickel show diverse applications as catalysts, magnetic recording media, conducting materials, and in medical diagnosis.[13] In the past decades, many different-shaped nickel nanocrystals, including nanotubes, hollow spheres, nanobelts, nanorods, and nanoprisms, have been successfully created and their properties and applications found to depend on their morphology.[7,14] Some of these assembled nickel nanostructures, such as microwires assembled by acicular nanocrystals and chains consisting of nanospheres, were created with the aid of surfactants or an external magnetic field.[11,15] However, the assembly mechanism has not been investigated thoroughly and to date little work has been reported on the synthesis of assembled nickel architectures by methods other than those mentioned above.

[a] Department of Chemistry, University of Science and Technology of China,
Hefei, Anhui 230026, People's Republic of China
Fax: +86-551-360-1600
E-mail: hgzheng@ustc.edu.cn
[b] State Key Lab of Fire Science, University of Science and Technology of China,
Hefei, Anhui 230026, People's Republic of China
Supporting information for this article is available on the WWW under http://www.eurjic.org or from the author.

In this manuscript we report a facile kinetic-control method for the preparation of wire-like assembled nanostructures of nickel that does not require surfactants or an external magnetic field. This synthetic methodology focuses on the modulation of the reaction rate to control the shapes of the building blocks and their spontaneous assembly behavior and has the advantage of being simple to perform and easy to control. The thus-prepared nickel wires with different-shaped subunits show variable magnetic properties and catalytic activity for the formation of carbon nanotubes in pyrolyzing acetone, depending on their microstructures.

Results and Discussion

Figure 1 shows a typical X-ray diffraction (XRD) pattern of sample1 (S1), in which all the diffraction peaks can be well indexed as ace-centered-cubic (fcc) nickel (JCPDS 01-1260). No peaks of nickel oxides or nickel hydroxides can be detected, thus indicating that pure fcc nickel is obtained by the current synthetic procedure.

The morphology of S1 is shown in Figure 2. The panoramic field emission scanning electron microscopy (FE-SEM) image in Figure 2 (a) indicates that the sample consists of reticular microwires with a diameter of about 2 μm and lengths of up to several hundred micrometers. The magnified images in parts b and c of Figure 2 demonstrate that the wires are prickly and are constructed from thorn-like particles with lengths of 200–400 nm. Figure 2 (d) is the TEM image of one wire and reveals the same characteristics as the SEM observations. Parts e, f and g of Figure 2 show a typical thorn-like subunit and the corresponding selected-area electron diffraction (SAED) and high-resolution TEM image. The pattern of spots reveals that the thorn is single-crystalline and the electron beam could be set along the

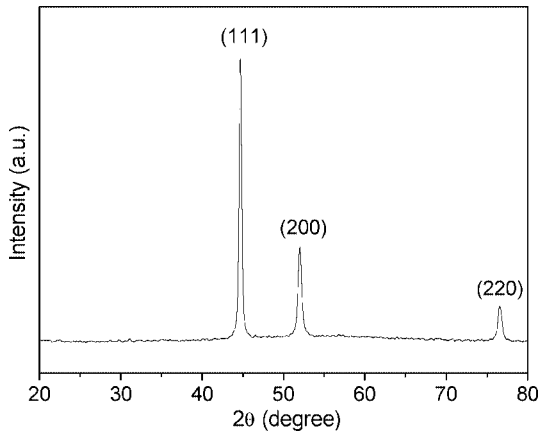

Figure 1. A typical XRD pattern of sample 1.

[$\bar{1}\bar{1}2$] zone axis. The spacing of the observed lattice planes is 0.20 nm, which is consistent with the separation of the (111) planes of fcc nickel. This demonstrates that the growth direction of the thorn is along the (111) plane. Analysis of several thorns gives a similar picture, thus suggesting that all the subunits have the same orientation.

In order to study the formation process of the wires, time-dependent TEM observations of the evolution of S1 were conducted; the results are shown in Figure 3. After 2 h, the product is present as small, granular nanocrystals with a diameter of 20–30 nm (Figure 3a). After heating the reaction mixture for 4 h thorns protrude from the particles and some prickly particles begin to aggregate due to their natural magnetic attraction, as shown in Figure 3b. After 8 h microwires consisting of thorn-like nanocrystals had formed (seen in Figure 3c). Figure 3d shows the HRTEM image recorded at the join of two neighboring subunits of the product heated for 8 h. It can be seen that the lattice

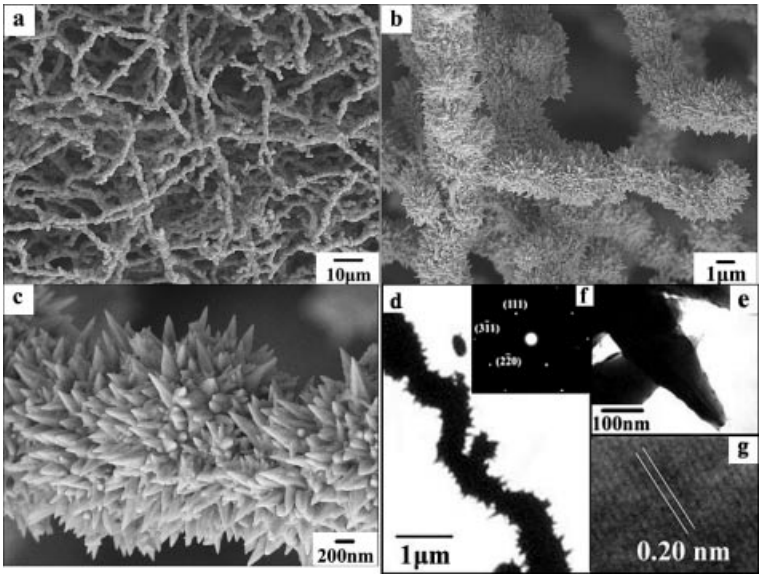

Figure 2. SEM and TEM images of sample 1: (a) a panoramic SEM image, (b) a low-magnification SEM image, (c) a high-magnification SEM image recorded on an individual wire, (d) a TEM image of a typical prickly wire, (e) a magnified TEM image of the thorn-like subunit, (f) the corresponding SAED image of the thorn, (g) the corresponding HRTEM image of the thorn.

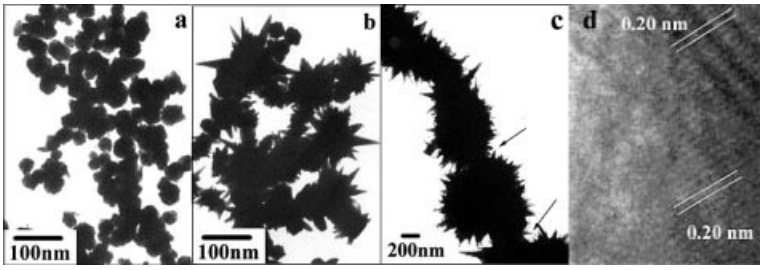

Figure 3. SEM images of the samples prepared at different reaction stages: (a) 2 h, (b) 4 h, (c) 8 h; (d) HRTEM image of the join of two neighboring thorn-like building blocks.

fringes prolongate across the two subunits without interruption by an apparent boundary, thus indicating that the building units have fused together. These results reveal that formation of the assembly wires occurs with a continuous aggregated growth rather than by direct aggregation of preformed, thorn-like particles.

Contrast experiments were carried out to investigate the factors that influence the formation of these nickel microwires. The redox reaction we employ here can be formulated as:

$$2\,[Ni(C_6H_5O_7)]^- + N_2H_4 + 4\,OH^- \rightarrow 2\,Ni + N_2 + 4\,H_2O + 2\,C_6H_5O_7^{3-}$$

Citrate was introduced here as the complexant to form the complex $[Ni(C_6H_5O_7)]^-$. Formation of this complex could sharply reduce the free Ni^{2+} concentration in solution and thus result in a relatively slow reaction rate, which is favorable for the oriented growth of nickel crystals.[16] To examine the effect of citrate ions on the formation of the wires, SEM images of the samples obtained at different molar ratios of citrate to Ni^{2+} ions (ω) were compared. In the absence of citrate, the reaction was complete after 30 min and the product consisted of irregular spherical particles (Figure 4, a). When ω was set to 0.5, where the amount of citrate is not sufficient to form the complex, the reaction time was prolonged to 4 h and the product was found to be a mixture of dispersed spherical particles and microwires (Figure 4, b). When ω was increased to 1.0, about 7 h was needed to complete the reaction and the product was dominated by microwires. These results indicate that citrate ions play a significant role in the formation of the wires.

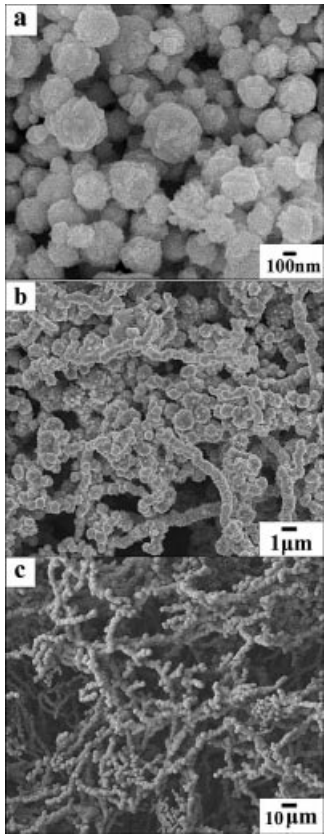

Figure 4. SEM images of the samples prepared at different molar ratios (ω) of citrate to Ni^{2+} ions: (a) ω = 0, (b) ω = 0.5, (c) ω = 1.0. The other reagent concentrations were kept the same.

The concentration of NaOH is another important parameter that affects the product morphology. It is known that a basic medium can increase the reducing power of hydrazine. Consequently, by adjusting the NaOH concentration, the reaction rate was correspondingly changed. Nickel wires were only obtained in a certain range of base concentrations when keeping the other conditions the same. Table 1 summarizes the reaction times and the product morphologies of the samples obtained at different base concentrations. The corresponding SEM images are shown in Figure 5. It can be seen that with an increase of base concentration the product gradually changes from wires into discrete particles and the reaction time is correspondingly shortened. A lower base concentration results in a relatively slow reaction rate, which facilitates the oriented growth of the nickel particles into thorns and their spontaneous assembly into wires. The fast reaction rate produced at high base concentrations only leads to bigger isolated particles.

The effect of temperature on the formation of the wires was also studied. It was found that the nickel wires could be fabricated in a wide temperature range of 70–140 °C. As the temperature decreases, the reaction time is obviously prolonged; for example, 2 h is sufficient to complete the reaction at 140 °C, while 36 h is needed for the reaction at 70 °C. No significant change of morphology and size was observed for the product obtained at different temperatures. In summary, an increase of reaction temperature accelerates the formation of the nickel wires but has little influence on their morphology and size.

Generally, nickel nanoparticles connect to each other due to magnetic interactions, although this magnetic dipole in-

Table 1. Reaction times and product morphologies of the samples prepared at different base concentration with the other conditions remaining the same.

Sample	NaOH conc. [M]	Reaction time [h]	Product morphology
1	0.05	10	microwires consisting of nanoplates (diameter of the wire: 2 μm)
2	0.10	8	microwires consisting of nanoplates (diameter of the wire: 1 μm)
3	0.15	5	microwires consisting of nanoparticles (diameter of the wire: 0.5 μm)
4	0.30	3	pearl-necklace-like microwires (diameter of the wire: 0.3 μm)
5	0.40	1	discrete particles with a diameter of 100 nm

teraction is rather weak and the aggregates can usually be dispersed by strong ultrasonication. Nevertheless, our wire-like assemblies show a high stability and even ultrasonication for 1 h could not destroy them. This indicates that the wire is not a loose aggregate of thorn-like nanocrystals but an integrated hierarchical structure. The assembly of magnetic particles is a complex process that is affected by several factors such as the velocity of crystal growth, dipolar interactions, spatial hindrance, and other kinetic factors. Based on the above studies of the evolution process and experimental parameters, the formation of our reticular hierarchical wires can be ascribed to the cooperative effect of the reaction rate and the inherent magnetic interactions. The reaction rate is controlled mainly by adjusting the reaction temperature and reagent concentration. During the first stage of the reaction spherical particles form as the nucleus. Then, anisotropic, thorn-like crystals develop from the active parts of the existing nuclei under the kinetic control of complexant and base and form prickly particles. Under the influence of the magnetic dipole interactions, the prickly particles tend to join with each other to acquire a low magnetic anisotropic energy. As the reaction proceeds, the contacting particles gradually fuse into each other and the separation between the joints disappears, which finally results in long wires. A schematic illustration of the possible formation process is presented in Scheme 1. During this process, there is a thermodynamic driving force for the aggregated growth because the surface energy is reduced substantially when the interface is eliminated.[17] As a result, reticular wires are observed.

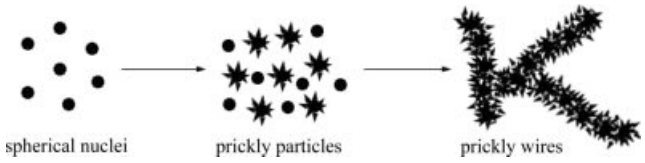

Scheme 1. Schematic illustration of the possible formation process of the prickly nickel microwires.

We have found that the diameter of the wire is not uniform and the narrower parts imply that the wires develop by the joining of discrete units. A relatively slow reaction rate is crucial for the formation of the thorn-like particles and their spontaneous aggregation into microwires. High base concentrations or low ω values lead to a high reaction rate, which means that the nucleus grows so fast into isolated spherical particles that oriented growth and simultaneous assembly essentially do not occur, while low base concentrations or high ω values allow a relatively slow reaction rate, which provides enough time for the oriented development of the nickel nuclei and their subsequent assembly. Such shape variations of nickel nanostructures with the basicity of the medium or complexant concentrations are the result of kinetic control of the crystal growth pro-

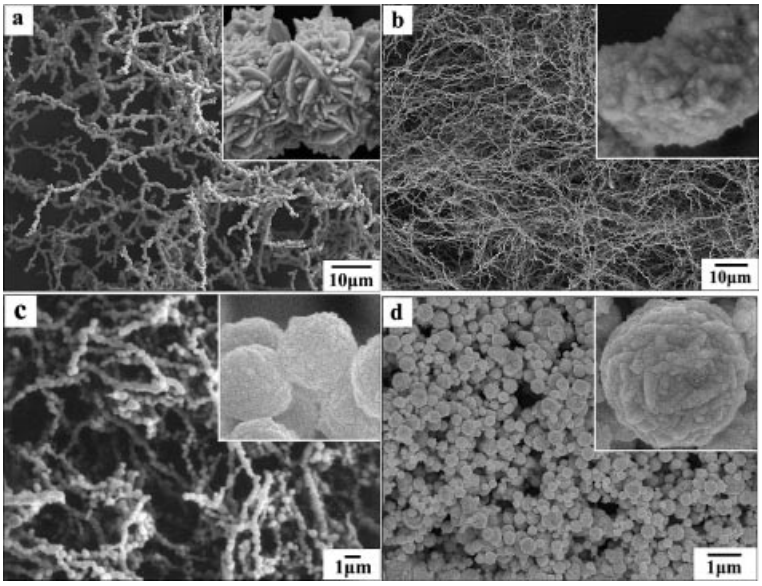

Figure 5. SEM images of the samples prepared at different NaOH concentrations: (a) 0.10 M, (b) 0.15 M, (c) 0.30 M, (d) 0.40 M. The other reagent concentrations were the same, namely $[NiCl_2]$ = 0.025 M, [citrate] = 0.10 M, $[N_2H_4]$ = 0.20 M.

cess. The wire formation observed within a specific range of base and complexant concentrations and temperatures therefore corresponds to an optimal combination of the reduction rate and crystal growth rate that allows organization of the building blocks.

In light of the formation mechanism proposed above, we conducted a series of experiments by replacing sodium citrate with other complexants such as sodium tartrate, sodium lactate, ethylenediamine, triethanolamine, and diethanolamine. In all cases we found similar results, namely that the base and complexant concentrations strongly influence the crystal morphology and assembly behavior. Wires with assembled nanostructures could only be reproducibly fabricated in a certain range of reagent concentrations. This result further proves the above aggregation growth mode, which is controlled by the complexant and inherent magnetic interactions. With the other conditions fixed, the base concentrations best suited to the formation of nickel wires in the presence of different complexants are summarized in Table 2 (their typical morphology images are given as Figure S1 in the Supporting Information).

Table 2. NaOH concentrations suitable for the formation of nickel microwires in the systems containing different complexants.[a]

Complexant	Conc. of complexant	Conc. of NaOH
Citrate	0.10 M	0.03–0.3 M
Tartrate	0.10 M	0.03–0.4 M
Lactate	0.10 M	0.06–0.2 M
Ethyleneamine	0.10 M	0.50–2.0 M
Triethanolamine	0.10 M	0.40–1.2 M
Diethanolamine	0.10 M	0.40–1.0 M

[a] The other reaction conditions were kept the same: $[NiCl_2]$ = 0.025 M, $[N_2H_4]$ = 0.2 M, hydrothermal treatment at 120 °C.

Magnetic Properties

It is known that the magnetic properties of nanomaterials are strongly dependent on their size, morphology, crystallinity, synthetic methods, etc. Four samples (samples 1, 2, 3, and 5) with different morphologies were selected as the subjects for investigation; their M-H hysteresis loops are presented in Figure 6. These samples show a coercivity (Hc) of 268, 257, 202, and 173 Oe, respectively. The corresponding saturation magnetism (Ms) is about 29.21, 27.36, 22.96, and 15.81 emu g^{-1}. All four samples show a much higher coercivity than bulk nickel (Hc = 100 Oe).[18] As ultrafine ferromagnetic particles often exhibit enhanced coercivity relative to the corresponding bulk material, the small size of the samples may be responsible for the increased Hc values.[19] The lower Ms values with respect to that of bulk nickel (55 emu g^{-1}) can be ascribed to the surface spin disorder and inevitable slight surface oxidation of the nanoscale subunits, which significantly reduce the total magnetic moments.[20] Moreover, it was found that the Hc and Ms values decrease gradually from sample 1 (S1) to sample 5 (S5) and that the wires with the thorn-like subunits have the highest Hc and Ms values, possibly due to the relatively higher shape anisotropy of their subunits.[21] This demonstrates that the microstructure of the samples greatly influences their magnetic properties, and the building blocks with higher shape anisotropy can effectively improve the magnetic properties of the assembly.

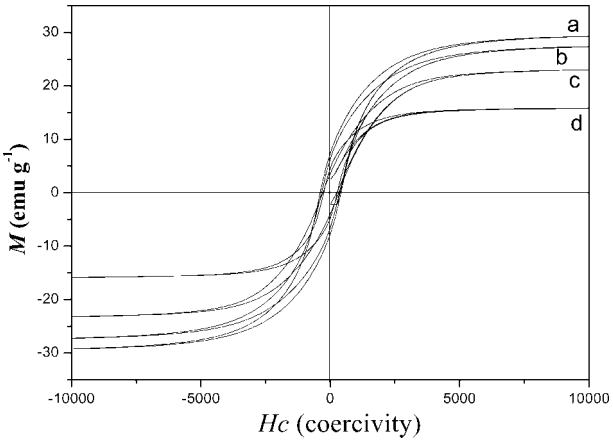

Figure 6. M–H hysteresis loops of four samples with different morphologies: (a) sample 1, (b) sample 2, (c) sample 4, (d) sample 5.

Catalytic Activity for the Formation of Carbon Nanotubes

Nickel is a commonly used catalyst for the formation of carbon particles.[22] Here, we studied the catalysis of the as-prepared nickel wires for the growth of carbon nanotubes in pyrolyzing acetone. Figure 7 shows the SEM and the corresponding TEM images of the obtained carbon particles catalyzed by S1–S5. In contrast to the product obtained without any metal particles, which appears as aggregated carbon particles without regular shapes (Figure 7, f), the five nickel samples all show catalytic activity for the creation of carbon nanotubes, but with different performances. Samples 1 and 2 both give carbon nanotubes with a yield of above 95% according to SEM observations (Figure 7, a, b). In the product catalyzed by sample 3 (S3), however, the yield of carbon nanotubes is only about 70% and some irregular particles are observed (seen in Figure 7, c). As for the reaction catalyzed by sample 4 (pearl-necklace-like chain), the yield of the tubes decreased to 40% and the length of the nanotubes obviously shortened (Figure 7, d). When it came to the reaction catalyzed by sample 5 (dispersed particles), much more irregular carbon particles were formed and only a few nanotubes (about 10%) could be detected, as seen in Figure 7 (e). These contrasting results clearly demonstrate that the catalytic activity of these nickel samples depends strongly on their microstructure. Since the structure and surface area of the catalyst are important factors affecting their activity, the samples with a relatively high surface area have more surface accessible to the reagents, which is believed contributive to their improved activity for the nucleation of carbon nanotubes,[23] although further research is needed to explore the detailed mechanism.

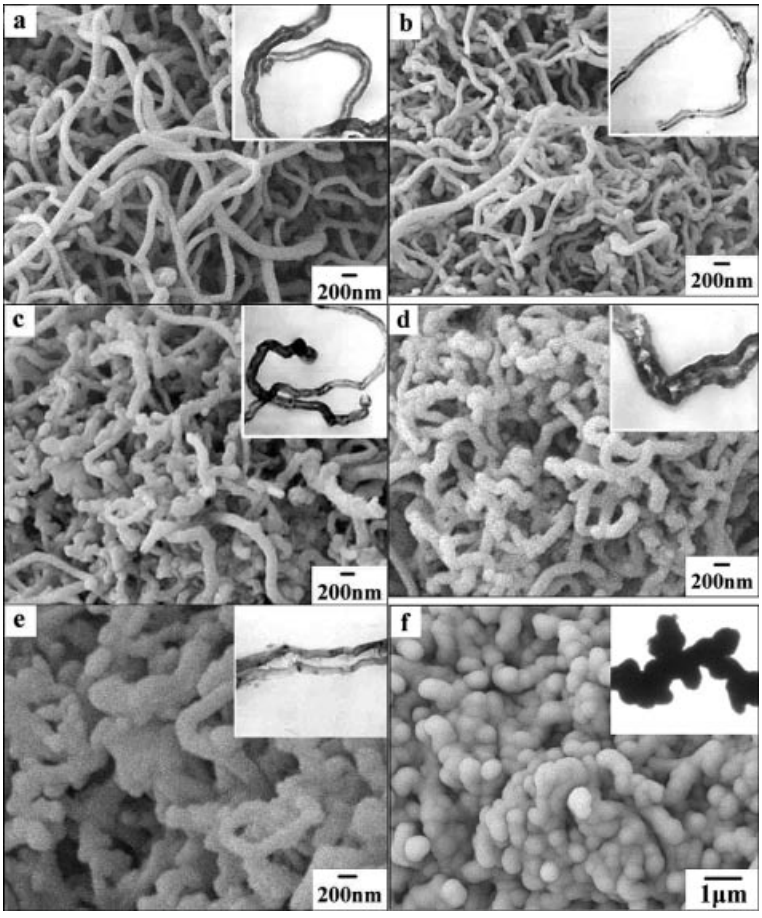

Figure 7. SEM images of the samples obtained in pyrolyzing acetone catalyzed by different nickel samples: (a) sample 1, (b) sample 2, (c) sample 3, (d) sample 4, (e) sample 5, (f) carbon particles fabricated without any nickel. The insets are the corresponding TEM images.

Conclusion

In summary, we have reported a simple complex-assisted hydrazine reduction method for the synthesis of hierarchical nickel microwires by controlling the reaction rate. The morphological details of the building blocks and their assembly behavior can be tailored by adjusting the reagent concentration. These nickel wires can be reproducibly created with the aid of various complexants, which proves the generality of this approach. The thus-prepared nickel wires show microstructure-dependent magnetic properties and catalytic activity for the growth of carbon nanotubes in pyrolyzing acetone, and they show superior magnetic properties and catalytic performance to the discrete particles. Our synthetic methodology is a facile route for assembling nanosized building blocks into desired structures through kinetic control that avoids the use of any surfactants or an external magnetic field. Such a method is expected to be extendable to the synthesis of other magnetic nanostructures.

Experimental Section

All chemicals were of analytical grade and were used without purification. A typical experiment for the preparation of nickel wires is as follows: trisodium citrate dihydrate ($Na_3C_6H_5O_7{\cdot}2H_2O$; 1.0 g) was dissolved in 30 mL of an aqueous solution of 0.025 M $NiCl_2$ whilst stirring. Then, 1.0 mL of hydrazine hydrate ($N_2H_4{\cdot}H_2O$ 80%) and a certain amount of dilute NaOH solution were added. The whole mixture was stirred for another 10 min to obtain a homogeneous solution and subsequently transferred into a 40-mL autoclave, which was sealed and maintained at 120 °C for 2–10 h. After the heating treatment was over, the black fluffy particles floating on the solution were collected, rinsed with distilled water and absolute ethanol, and finally dried under vacuum. The samples obtained at NaOH concentrations of 0.05, 0.10, 0.15, 0.30, and 0.40 M are denoted as samples 1 (S1), 2 (S2), 3 (S3), 4 (S4), and 5 (S5), respectively.

For the synthesis of carbon particles, 20 mg of the thus-prepared nickel sample was added to two 20-mL stainless autoclaves containing 12 mL of acetone. The autoclave was then sealed, heated at a rate of 5 °C min^{-1} to 550 °C, and kept at this temperature for 10 h. After the heating treatment was over, the autoclave was cooled naturally to room temperature and the black precipitates were collected and immersed in dilute HNO_3 solution whilst stirring for 12 h. The product was then centrifuged, rinsed with distilled water and absolute ethanol, and finally vacuum dried at 50 °C for 2 h.

X-ray diffraction (XRD) patterns of the samples were recorded with a Philips X′pert diffractometer with Cu-K_α radiation (λ = 1.5418 Å). The morphology and structure of the sample were studied by field emission scanning electron microscopy (FE-SEM, JEOL JSM-6300F) and transmission electron microscopy (TEM, Hitachi, H-800) with an accelerating voltage of 200 kV. High-reso-

lution TEM images were recorded with a JEOL-2010 TEM at an acceleration voltage of 200 kV. Magnetization–hysteresis (M-H) loops were recorded with a BHV-55 vibrating sample magnetometer (VSM) at room temperature.

Supporting Information (see also the footnote on the first page of this article): SEM images of the samples prepared with the assistance of different complexing agents (Figure S1).

[1] S. H. Sun, C. B. Murray, D. Weller, L. Folks, A. Moser, *Science* **2000**, *287*, 1989–1992.

[2] a) B. Z. Tang, Y. H. Geng, J. W. Y. Lam, B. S. Li, X. B. Jing, X. H. Wang, F. S. Wang, A. B. Pakhomov, X. X. Zhang, *Chem. Mater.* **1999**, *11*, 1581–1589; b) M. Kryszewski, J. K. Jeszka, *Synth. Met.* **1998**, *94*, 99–104; c) V. F. Puntes, P. Gorostiza, D. M. Aruguete, N. G. Bastus, A. P. Alivisatos, *Nat. Mater.* **2004**, *3*, 263–268; d) M. Bruchez, M. Moronne, P. Gin, S. Weiss, A. P. Alivisatos, *Science* **1998**, *281*, 2013–2016.

[3] a) R. P. Andres, J. D. Bielefeld, J. I. Henderson, D. B. Janes, V. R. Kolagunta, C. P. Kubiak, W. J. Mahoney, R. G. Osifchin, *Science* **1996**, *273*, 1690–1693; b) J. Jin, T. Iyoda, C. Cao, Y. Song, L. Jiang, T. J. Li, D. B. Zhu, *Angew. Chem. Int. Ed.* **2001**, *40*, 2135–2138; c) F. Caruso, R. A. Caruso, H. Mohwald, *Science* **1998**, *282*, 1111–1114; d) C. A. Mirkin, R. L. Letsinger, R. C. Mucic, J. J. Storhoff, *Nature* **1996**, *382*, 607–609.

[4] Y. L. Hou, S. Gao, T. Ohta, H. Kondoh, *Eur. J. Inorg. Chem.* **2004**, 1169–1173.

[5] L. E. Euliss, S. G. Grancharov, S. O'Brien, T. J. Deming, G. D. Stucky, C. B. Murray, G. A. Held, *Nano Lett.* **2003**, *3*, 1489–1493.

[6] S. H. Sun, S. Anders, H. F. Hamann, J. U. Thiele, J. E. E. Baglin, T. Thomson, E. E. Fullerton, C. B. Murray, B. D. Terris, *J. Am. Chem. Soc.* **2002**, *124*, 2284–2285.

[7] N. Cordente, R. M. Espaud, F. Secocq, M. J. Casanove, C. Amies, B. Chaudret, *Nano Lett.* **2001**, *1*, 565–568.

[8] M. Tanase, L. A. Bauer, A. Hultgren, D. M. Silevitch, L. Sun, D. H. Reich, P. C. Searson, G. J. Meyer, *Nano Lett.* **2001**, *1*, 155–158.

[9] E. V. Shevchenko, D. V. Talapin, A. L. Rogach, A. Komowski, M. Haase, H. Weller, *J. Am. Chem. Soc.* **2002**, *124*, 11480–11485.

[10] Y. Sahoo, M. Cheon, S. Wang, H. Luo, E. P. Furlani, P. N. Prasad, *J. Phys. Chem. B* **2004**, *108*, 3380–3383.

[11] S. Singamaneni, V. Bliznyuk, *Appl. Phys. Lett.* **2005**, *87*, 162511.

[12] W. X. Zhang, C. B. Wang, H. L. Lien, *Catal. Today* **1998**, *40*, 387–395.

[13] a) V. F. Puntes, K. M. Krishnan, A. P. Alivisatos, *Science* **2001**, *291*, 2115–2117; b) R. Hernandez, S. Polizu, S. Turenne, L. Yahia, *Bio-Med. Mater. Eng.* **2002**, *12*, 37–45; c) A. Smogunov, A. Dal Corso, E. Tosatti, *Surf. Sci.* **2002**, *507*, 609–614.

[14] a) J. S. Bradley, B. Tesche, W. Buser, M. Maase, M. T. Reetz, *J. Am. Chem. Soc.* **2000**, *122*, 4631–4636; b) J. Bao, C. Tie, Z. Xu, Q. Zhou, D. Shen, Q. Ma, *Adv. Mater.* **2001**, *13*, 1631–1633; c) J. Bao, Y. Liang, Z. Xu, L. Si, *Adv. Mater.* **2003**, *15*, 1832–1835; d) Z. Liu, S. Li, Y. Yang, S. Peng, Z. Hu, Y. Qian, *Adv. Mater.* **2003**, *15*, 1946–1948; e) X. M. Ni, Q. B. Zhao, H. G. Zheng, B. B. Li, J. M. Song, D. E. Zhang, X. J. Zhang, *Eur. J. Inorg. Chem.* **2005**, 4788–4793.

[15] a) H. Niu, Q. Chen, M. Ning, Y. Jia, X. Wang, *J. Phys. Chem. B* **2004**, *108*, 3996–3999; b) C. M. Liu, L. Guo, R. M. Wang, Y. Deng, H. B. Xu, S. H. Yang, *Chem. Commun.* **2004**, 2726–2727.

[16] S. M. Lee, Y. W. Jun, S. N. Cho, J. Cheon, *J. Am. Chem. Soc.* **2002**, *124*, 11244–11245.

[17] A. P. Alivisatos, *Science* **2000**, *289*, 736–737.

[18] L. Guo, C. M. Liu, R. M. Wang, H. B. Xu, Z. Y. Wu, S. H. Yang, *J. Am. Chem. Soc.* **2003**, *126*, 4530–4531.

[19] J. H. Hwang, V. P. Dravid, M. H. Teng, J. J. Host, B. R. Elliott, D. L. Johnson, T. O. Mason, *J. Mater. Res.* **1997**, *12*, 1076–1082.

[20] D. L. L. Pelecky, R. D. Rieke, *Chem. Mater.* **1996**, *8*, 1770–1783.

[21] S. H. Wu, D. H. Chen, *J. Colloid Interface Sci.* **2003**, *259*, 282–286.

[22] a) E. F. Kukovitsky, S. G. L'vov, N. A. Sainov, V. A. Shustov, *Appl. Surf. Sci.* **2003**, *215*, 201–208; b) H. Gao, J. Lin, H. Pan, G. Wu, Y. Feng, *Chem. Phys. Lett.* **2004**, *393*, 511–516; c) M. Han, W. Zhang, C. Gao, Y. Liang, Z. Xu, J. Zhu, J. He, *Carbon* **2006**, *44*, 211–215.

[23] C. Phan-Huu, R. Vieira, B. Louis, A. Carvalho, J. Amadou, T. Dintzer, M. J. Ledoux, *J. Catal.* **2006**, *240*, 194–202.

Received: September 9, 2006
Published Online: November 29, 2006

